Cite as Lannoeye, W., Stal, C., Guyassa, E., Zenebe, A., Nyssen, J., Frankl, A., 2016. The use SfM-photogrammetry to quantify and understand gully degradation at the temporal scale of rainfall events: an example from the Ethiopian drylands. Physical Geography, 37(6): 430-451. DOI 10.1080/02723646.2016.1234197.

The use SfM-photogrammetry to quantify and understand gully degradation at the temporal scale of rainfall events: an example from the Ethiopian drylands

Wouter Lannoeye[1,*], Cornelis Stal[1], Etefa Guyassa[1,2], Amanuel Zenebe[2], Jan Nyssen[1], Amaury Frankl[1,3]

[1] Department of Geography, Ghent University, Krijgslaan 281 (S8), B-9000 Gent, Belgium

[2] Department of Land Resource Management and Environmental Protection, Mekelle University, P.O. Box 231, Mekelle, Ethiopia

[3] Research Fund – Flanders (FWO), Egmontstraat 5, B-1000 Brussels, Belgium

* Corresponding author: e-mail: wouterlannoeye@gmail.com, phone: +32471466537, address: Krijgslaan 281 (S8), B-9000 Ghent, Belgium.

Cite as Lannoeye, W., Stal, C., Guyassa, E., Zenebe, A., Nyssen, J., Frankl, A., 2016. The use SfM-photogrammetry to quantify and understand gully degradation at the temporal scale of rainfall events: an example from the Ethiopian drylands. Physical Geography, 37(6): 430-451. DOI 10.1080/02723646.2016.1234197.

ABSTRACT

With the recent technological advances offered by SfM-photogrammetry, we now have the possibility to study gully erosion at very high spatial and temporal scales from multi-temporal DEMs; and thus to enhance our understanding of both gully erosion processes and controls. Here, we exanimate erosion gully degradation and aggradation at the gully head cut and at four re-incisions along the gully reach (Northern Ethiopia). Environmental controls recorded are topography rainfall, runoff, land use and cover, land management and soil characteristics; revealing that the overall vulnerability of the catchment to erosion is low as calculated from the RUSLE (average 11.83 ton ha^{-1} y^{-1}). This reflects the successful land management of the past years. The runoff coefficient was on average 7.3% (maximum of 18.2%). Runoff events caused most geomorphic change in the gullies, but slumping of the gully bank also occurred on dry days. Most geomorphic change was caused by one major rainfall event of 54.8 mm d^{-1}, and smaller runoff events caused both degradation and aggradation, often asynchronous between studied sites. Important is that although most research focuses on gully heads alone, re-incisions at lower locations can still cause important gully degradation, which ultimately will reach the gully head and cause instability.

Keywords: Digital Elevation Model (DEM), Gully head cut, Multi-temporal, PhotoScan, Revised Universal Soil Loss Equation, Volume.

Cite as Lannoeye, W., Stal, C., Guyassa, E., Zenebe, A., Nyssen, J., Frankl, A., 2016. The use SfM-photogrammetry to quantify and understand gully degradation at the temporal scale of rainfall events: an example from the Ethiopian drylands. Physical Geography, 37(6): 430-451. DOI 10.1080/02723646.2016.1234197.

1. Introduction

Gully erosion is one of the most important soil degradation processes in a wide range of environments (Valentin, Poesen & Li, 2005), causing considerable soil losses (Poesen, Nachtergaele, Verstraeten & Valentin, 2003). Numerous causes are mentioned in literature to explain accelerated erosion by gullying, such as deforestation, agricultural intensification, overgrazing, urbanization and flow diversion by infrastructure (Schumm, 2005). In drylands, gully erosion is often related to vegetation cover degradation, flow diversion and climatic change. Although the concern for gully erosion has strongly increased over the past decade (e.g., Hu et al., 2007; Ndona & Truong, 2011; d'Oleire-Oltmanns, Marzolff, Castillo, Pérez, James, Quinton, Targuas & Gómez, 2012; Peter & Ries, 2012; Peter *et al.*, 2014; Frankl et al., 2015; Stöcker, Eltner & Karrasch, 2015), understanding gully erosion processes whilst integrating environmental controls at fine spatio-temporal scales is generally lacking.

Parallel to technological advances, methods for measuring morphological changes of gullies have rapidly developed and diversified. Classical approaches are commonly based on measuring in-situ using a tape meter (Oostwoud Wijdenes & Bryan, 2001) or a theodolite (Nyssen et al., 2006); and later using Global Navigation Satellite System (GNSS) receivers (Wu & Cheng, 2005; Hu et al., 2007). Aerial photographs, usually available since the early to mid 20th century for many regions worldwide, also proved to benefit gully erosion studies, especially since Digital Elevation Models (DEMs) derivates allow to quantify gully networks, particularly when large-scale photographs are available (Burkard and Kostaschuk, 1995, 1997; Oostwoud-Wijdenes, Poesen, Vandekerckhove, Nachtergaele & De Baerdemaeker, 1999; Betts, Trustrum & Rose, 2003). In the late 20th century, with the launching of very high resolution satellite imagery, aerial photographs were mostly substituted by high resolution satellite imagery (Quénéhervé, Bachofer & Mori, 2015). Quantifying gully morphology in a direct way at very high spatial resolutions became possible with the use of laser scanning, both from terrestrial (Bonilla et al., 2008; Perroy, Bookhagen, Asner & Chadwick, 2010; Kociuba, Janicki & Rodzik, 2014), and airborne approaches (Heritage and Hetherington, 2007; Perroy et al., 2010). Despite the fine resolutions at which gullies can be studied, the above mentioned methods often suffer from high cost and/or low flexibility, which can hamper research especially when high temporal resolutions are required to truly understand erosion dynamics. A recent low-cost method that has been applied in gully erosion studies is Structure-from-Motion (SfM) photogrammetry which allows producing DEMs at very high spatio-temporal resolutions.

Cite as Lannoeye, W., Stal, C., Guyassa, E., Zenebe, A., Nyssen, J., Frankl, A., 2016. The use SfM-photogrammetry to quantify and understand gully degradation at the temporal scale of rainfall events: an example from the Ethiopian drylands. Physical Geography, 37(6): 430-451. DOI 10.1080/02723646.2016.1234197.

SfM-photogrammetry is an innovative method that allows to rapidly obtain accurate (mm to cm-level) data on gully morphologies and dynamics (Frankl et al., 2015). Data acquisition is more flexible and cost-efficient than earlier mentioned methods since it does not require specific equipment besides a digital photograph camera, a computer laboratory (workstation) and measuring equipment for establishing a network of Ground Control Points (GCPs). In recent years, SfM-photogrammetry was introduced in earth-science research (Smith, Carrivick & Quincey, 2015), for example to study of moraines (Westoby, Brasington, Glasser, Hambrey & Reynolds, 2012), lava domes (James & Varley, 2012), landslide displacements (Lucieer, de Jong & Turner, 2013; Rothmund, Niethammer, Malet & Joswig, 2013), coastal change (James, Ilic & Ruzic, 2013), braided rivers (Javernick, Brasington & Caruso, 2014) and gully erosion (Castillo et al., 2012; James & Varley, 2012; d'Oleire-Oltmanns et al., 2012; Gómez-Gutiérrez et al., 2014; Kaiser et al., 2014; Peter, d'Oleire-Oltmanns, Ries, Marzolff & Hssaine, 2014; Frankl et al., 2015). In these studies, Unmanned Aerial Vehicles (UAVs) were frequently used for photographing large areas covered by the surveyed landforms.

This study aims to explore the use SfM-photogrammetry to quantify and understand gully degradation at high spatial resolutions and at very short time intervals, i.e. at the temporal scale of rainfall events. From this, we aim at enhancing our understanding of the causal relationships between gully erosion processes and environmental controls and overall catchment erosion vulnerability at the scale of small gully catchments, allowing to improve the planning of soil and water conservation interventions. A case study was developed for a gully catchment in Northern Ethiopia.

2. Materials and Methods

2.1 Study area

The study area consists of a steep-sloped small gully catchment located on a high mountain slope (2365 – 2505 m a.s.l.) in the Ethiopian Highlands (Figure 1), at the rural village of Adi Kolkwal (13°39N, 39°12E). The stepped topography of the Ethiopian Highlands (*Amba* landscape) reflects the subhorizontal geological structure in the region (Nyssen, Poesen, Moeyersons, Deckers, Mitiku & Lang, 2004b), comprising of Mesozoic Antalo limestone overlain by Amba Aradan sandstone and Tertiary basalt flows. The study area is topographically marked by a sandstone escarpment at ca. 2550 m a.s.l.. On top of the basalt or basaltic colluvium, Vertisols are found. Leptosols are located near cliffs, Regosols and

Cite as Lannoeye, W., Stal, C., Guyassa, E., Zenebe, A., Nyssen, J., Frankl, A., 2016. The use SfM-photogrammetry to quantify and understand gully degradation at the temporal scale of rainfall events: an example from the Ethiopian drylands. Physical Geography, 37(6): 430-451. DOI 10.1080/02723646.2016.1234197.

Cambisols occur on steep slopes, and near the foot slope, finer textured soils are found (Vertisol) (Frankl et al., 2012).

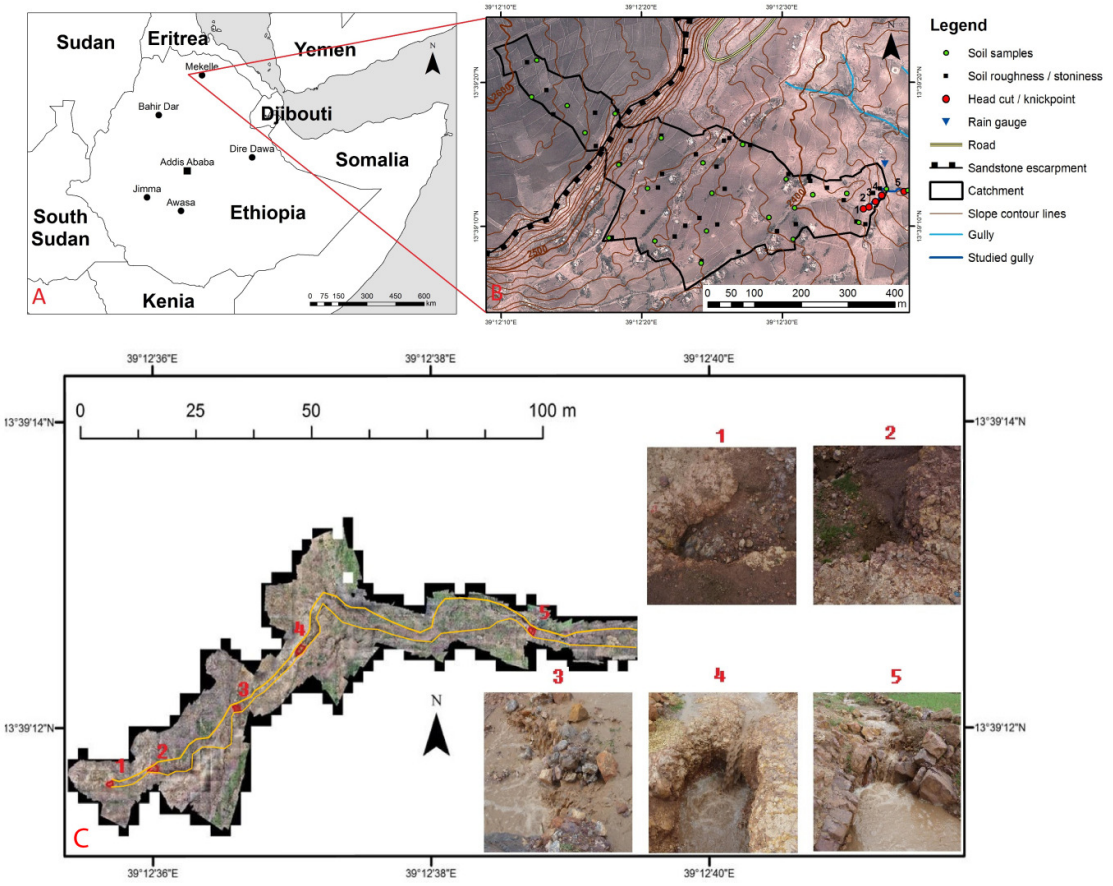

Figure 1: Location of the studied catchment in Ethiopia (A), detailed view on the catchment and measurement locations (B) and orthophotograph of the gully with the 5 erosion sites studied (C): head cut (site 1) and re-incisions (sites 2-5) (red) within the gully banks (orange lines). A full model of the gully was built on low resolution to create an overview of the gully. As can be seen from several photographs, plunge pools are present at the re-incisions.

About 33% of the Northern Ethiopian Highlands is cropland (Meire et al., 2013; de Mûelenaere et al., 2012). Nearly all this land is cultivated by smallholders who each have about a hectare (Gebremedhin & Swinton, 2003), and produce food following traditional practices for their subsistence or for the local market (Lanckriet et al., 2014). Crop production is primarily based on rainfed agriculture. With the rapid population growth in the second half

of the 20th century and early 21th century a sharp increase in food production needs occurred, increasing the pressure on natural resources (FAO, 2011).

The overall low vegetation cover in Northern Ethiopia is the result of deforestation (Nyssen et al., 2004b) and overgrazing (Frankl et al., 2012). Over the past decades, measures have been taken to reduce soil degradation which include establishing exclosures, terracing slopes and the construction of check dams in gullies (Nyssen et al., 2004b) to protect the cropland, which is the main land use, against further degradation.

The climate is semi-arid and has an erratic rainy season from June to September driven by the position of the Inter Tropical Convergence Zone (Robinson & Henderson-Sellers, 1999). The annual precipitation in the nearby (1-2 km) May Zeg Zeg catchment is on average 774 mm y^{-1} (Nyssen et al., 2009) which falls as intense rain showers seldom lasting longer than 10 minutes (Nyssen et al., 2005). Clouds generally form in the morning as a result of evaporation and convective cloud formation and rain starts in the afternoon. Rainfall is unpredictable in this region with a great number of days during the rainy season with very little to no rainfall. The median drop diameters, up to 4.4 mm (± 9.88 mm) at a rainfall intensity of 72 mm h^{-1}, are larger than those found in other regions around the world, causing high rain erosivity (Nyssen et al., 2005). Eighty-eight percent of the rainfall falls with intensities < 30 mm h^{-1} (Nyssen et al., 2005).

This specific gully was chosen for its good accessibility and because the catchment is a good representation of a large number of catchments in the Northern Ethiopian highlands. Specific catchment characteristics will be presented in the results section.

2.2 Assessing the erosion vulnerability of the catchment

In order to assess the erosion vulnerability of the catchment after years of intensified soil and water conservation efforts and the impact of environmental factors on gully erosion rates, relevant catchment characteristics were quantified, including topography rainfall, runoff, land use and cover, land management and soil characteristics. Positional information was gathered using a Garmin eTrex 30 GNSS. This is a WAAS-capable receiver with a 2 m accuracy computed in real-time.

The catchment was delimited from field observations taking surface drainage patterns into account. This was done shortly after rainfall events and has the advantage of reducing delineation errors in a landscape where humans strongly interfere with surface hydrology. Five-minute rainfall depth was measured near the study area using an automatic tipping-

bucket rain gauge having an accuracy of 2 mm. From this, 1-hour rainfall intensity and daily rainfall depth were calculated. Catchment runoff was measured using a V-notch that was constructed in the gully at the catchment outlet. Runoff stage height was measured with an Eijkelkamp automatic e+ WATER L sensor (resolution level of 1 mm and accuracy level of 5 mm, time interval of 1 minute), and converted into discharge by Dinssa et al. (2015).

Land use was mapped, and since this mainly considered cropland, crop type and growth was monitored per plot during the crop growing season; from observations on 1 and 15 August and 1 September. Both average crop height and crop cover were measured on locations at least 2 m from the plot border. Average crop height was measured in each field using a tape meter. Crop cover was determined from vertical photographs taken in the field using a Sony Nex-5R with a fixed 20 mm camera lens. For the 93 plots of cropland in the catchment, two photographs were taken from the same height and were cropped to 1 m² Adobe Photoshop. The crop cover was determined from a colour range selection of greens in Adobe Photoshop, successfully tested on multiple photographs with a wide range of greens. Selection criteria for this were (range): Luminance (20.63 - 89.18), A (-31.91 to -14.37) and B (17.45 - 62.27) (the A channel provides information about greens and magentas, the B channel provides information about yellows and blues). Average values from both photographs per site were considered for the crop cover of that field.

Tillage direction of every plot was determined by following a representative furrow whilst taking GPS-points. Tillage direction was compared to the average orientation of the topographical contour lines. Stone bunds were mapped.

Soil roughness and stoniness were determined from 37 randomly distributed locations on cropland (Figure 1). This was done at the beginning of the rainy season and using image-based modelling (Thomsen, Stolte, Baartman & Starkloff, 2014), in PhotoScan. Between the moment of ploughing and the soil roughness determination, two rainfall events occurred – slightly smoothening the surface – after which we assumed that the soil roughness did not change significantly during the rainy season. This assumption is supported by the rapid average crop growth of 200 mm in the first month after sowing, which protects the soil from further smoothening due to rainfall. Marked rock fragments were placed on the soil surface to outline 1 m². In order to remove the slope effect during the roughness calculation, the elevation of the marked corner points were all set to one during the processing in PhotoScan (and subsequently removed by cropping). The random soil roughness was determined by extracting the standard deviation of the 1 m² plots from the DEMs. Soil stoniness was

determined from a point count method using draped DEMs. A raster of 100 cells with a 5 x 5 mm cell size, representing the actual soil surface area (Soil Survey Division Staff, 1993), was therefore superposed on the draped DEMs.

Soil bulk density and texture were measured on 7 and 8 August by randomly sampling 26 undisturbed soil samples (1.73 samples ha^{-1}; Figure 1) using Kopecky rings with a volume of 100 cm^3. All samples were taken in tillage furrows and several meters from cropland margins. The samples were oven-dried for 24 hours at 105°C and weighted to calculate the soil bulk density. The soil texture was determined by wet sieving and using a Sedigraph III Plus (Micromeritics), to determine the fractions of sand, silt and clay.

To extrapolate randomly distributed point measurements to the entire catchment, the inverse distance weighted method was used; the further a point is removed from the sample, the less influence it has in the averaging process. In this case, the influence by distance decayed with a power of 2.

Assessing the erosion sensitivity of the catchment was done by calculating the yearly soil loss rate on a 25 x 25 m grid, using the Revised Universal Soil Loss Equation (RUSLE). The RUSLE was calibrated by Nyssen et al. (2009) for the nearby (1-2 km) May Zegzeg catchment, and we adopted in according to the results in this study (e.g. P-values between 0.85 and 0.9 were used here due to a larger range of soil roughness in the catchment).

2.4 Quantifying gully head retreat rates

2.4.1 Field data collection

Field data collection occurred in Ethiopia during the rainy season (July-September) of 2014. Before the data collection could start, the sparse vegetation in and near the gully was clipped to the ground level in order to capture the real topography. As vegetation was rather scarce and only the above ground vegetation was removed, this presumably had limited impact on erosion dynamics. Other preliminary work included marking a set of permanent Ground Control Points (GCP). Therefore, paint marks were applied on large rocks in and around the gully. The GCPs were measured using a Sokkia Set 550x total station, with an accuracy of 2 cm. For the absolute orientation, two GCPs were localized with a Garmin eTrex 30 GNSS (2 m standard deviation). The relative orientation of all the GCPs was, however, most essential here given that temporal DEMs were studied.

To monitor gully head retreat rates at very high spatio-temporal scales, a SfM-Multi-View-Stereo (MVS) modelling workflow was used in the image-based modelling software package

PhotoScan by Agisoft (Figure 2; Remondino & El-Hakim, 2006; Verhoeven , 2011; Westoby et al., 2012; Gómez-Gutiérrez et al., 2014; Javernick et al., 2014; Frankl et al., 2015). SfM-MVS has the advantage over conventional photogrammetry that a large series of photographs are instantaneously used for the virtual reconstruction of the scene, instead of stereographs for each consecutive couple.

The collection of photographs for the SfM-MVS method was done with a Sony Nex-5R with a fixed 20mm lens. This camera has an APS-C sensor with 16.1 megapixels and a sensor size of 25.1 x 16.7 mm. Photographs were taken under diffuse light conditions (i.e. clouded sky), in order to reduce the impact of casted shadows on photograph contrast. The photographing of the gully took place after every rainfall event with runoff which implied photographing had to be finished before the rains that regularly occur in the afternoon. Photographing started at dawn and the time needed to photograph the gully varied between 1 hour 40 minutes and 5 hours 15 minutes, depended on the duration of the clouded periods during the day.

Up to August 6, all the photographs were made on eye level. Thereafter, the camera was mounted onto a small platform on top of a 5 m wooden pole which delivered vertical photographs (Figure 3). The change in method had a positive effect on the number of photographs that could be aligned during model construction. No flash or specific settings for the camera were used, only the optimal settings for that day which ensured sharp photographs with good contrast.

2.4.2 SfM-photogrammetic workflow

In this research, PhotoScan (Agisoft version 1.0.2) was used to execute the workflow for SfM-MVS modelling presented in Figure 2. Since the aim of this research was to acquire very detailed data on gully erosion dynamics, the settings for all the steps in SfM-MVS modelling were set to the highest quality. Other settings resulted in a surface not well representing reality. The choice for high quality settings impeded the creation of 3D models in our computer laboratory (4-core Intel i7 processor at 3.70GHz, 32GB RAM and GeForce GTX 780 3GB RAM graphics card, Microsoft Windows 7 64-bit) due to the minimum memory requirements suggested by the software manufacturer. Furthermore, manual editing in PhotoScan was necessary for fine-tuning the model, deletion of erroneous points and quality control (Frankl et al., 2015).

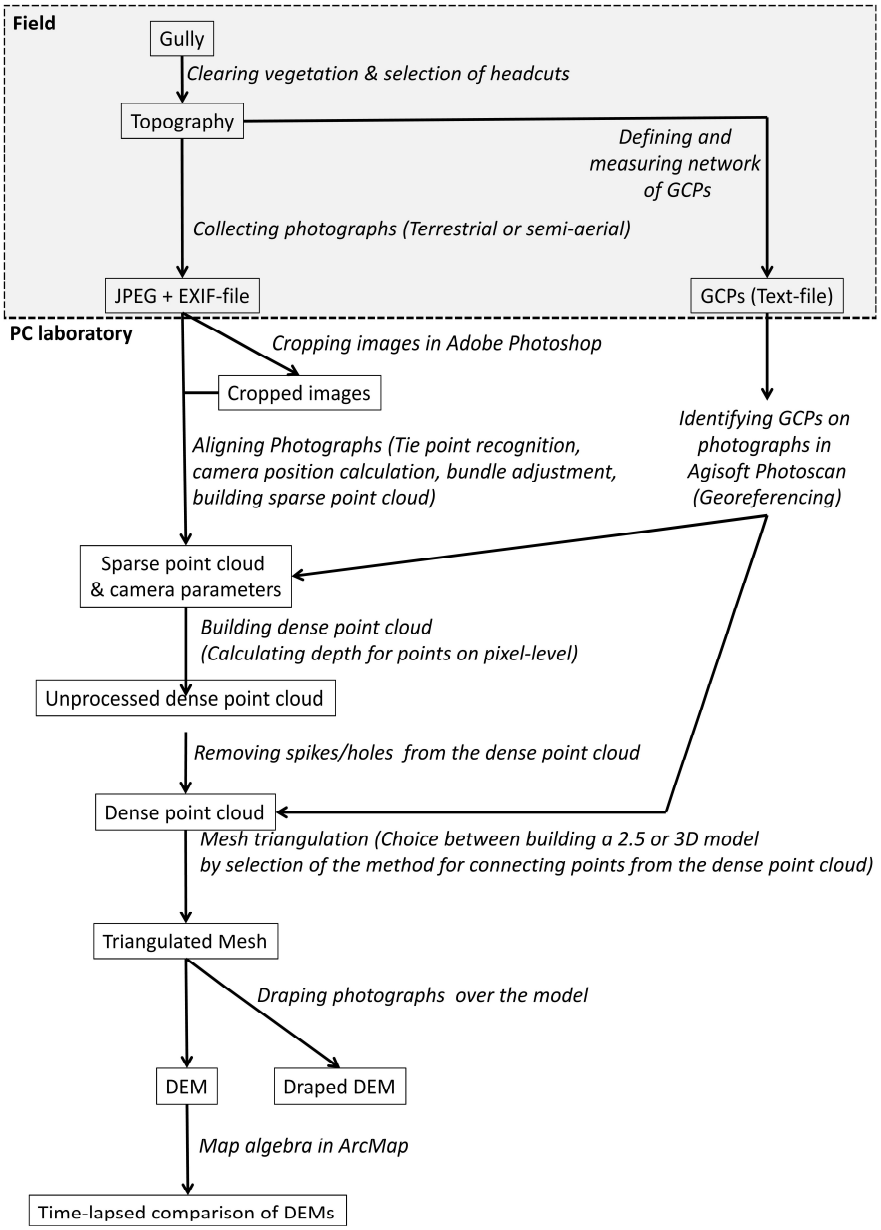

Figure 2: Workflow of SfM-MVS modelling, differentiating between data collection in the field (grey background) and the computer based modelling (white background).

Before importing the photographs into PhotoScan, the vertical photographs were cropped in Adobe Photoshop to remove the part of the photograph containing the wooden pole on which the camera was mounted. The same result could be achieved by masking a part of the photographs in PhotoScan. Once the photographs were imported in PhotoScan, the GCPs were identified for georeferencing the result of the SfM-MVS modelling. The workflow was semi-automated, since the identification of GCPs was performed manually. The first step in

the modelling sequence is SfM-aligning the photographs by image triangulation based on the recognition of points occurring in two or more photographs. This creates a scene estimation consisting of a sparse point cloud and a reconstruction of the camera configurations during the acquisition. The MVS-step results in a dense point cloud by calculating the depth information for the pixels in the aligned photographs. For some models, the dense point cloud was edited to exclude points with an incorrect depth calculation from further processing. The last step before finalizing the model is to build a triangular mesh in order to obtain a closed surface. This is the phase where a distinction between full 3D and 2.5D modelling is required. In this study, the choice was made for 2.5D modelling to reduce the computation time (one z-value per xy-coordinate pair).

In total, 125 DEMs models were produced, based on ca. 40 photographs per model. The accuracy of models depends on the distance between the photographer and the surveyed feature (equivalent of the height in conventional photogrammetry) and the distance between consecutive photographs (equivalent of the baseline). Furthermore, an important factor of model quality is the GCP distribution. The accuracy of the DEMs, computed from a least-square adjustment of the 9 GCPs used for the error calculation, was 2 cm.

Cite as Lannoeye, W., Stal, C., Guyassa, E., Zenebe, A., Nyssen, J., Frankl, A., 2016. The use SfM-photogrammetry to quantify and understand gully degradation at the temporal scale of rainfall events: an example from the Ethiopian drylands. Physical Geography, 37(6): 430-451. DOI 10.1080/02723646.2016.1234197.

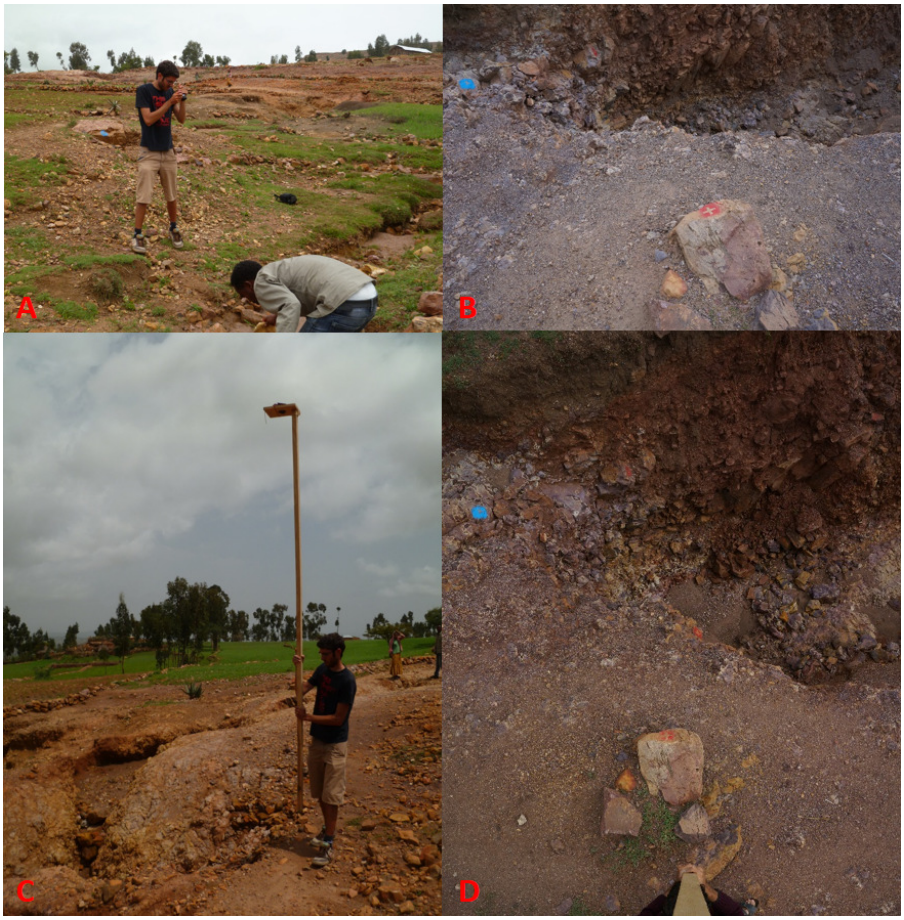

Figure 3: Photographing for SfM-photogrammetry. A) Terrestrial photography and B) resulting photograph. C) Camera mounted on a platform on top of a wooden pole and D) resulting photographs (each covering an area of approximately 4 to 9 m²).

2.4.3 Quantifying erosion rates

From field observations on gully erosion dynamics during the rainy season, we observed that most geomorphic change occurred at gully knick points, i.e. the gully head and re-incisions in the gully floor. Other parts of the gully showed no signs of active erosion processes. In addition, limiting the monitoring sites had the advantage of strongly reducing processing time. Five segments were eventually retained for detailed study: the gully head and four re-incisions (Figure 1). For each, 25 temporal DEMs were produced (= number of rainfall events with runoff, not necessarily reaching runoff sensor at the V-notch further in the gully). The studied segment were subtracted from each other to obtain a DEM which represents the differential gully topography between two subsequent rainfall events. The DEMs were numbered according to their temporal sequence during the rainy season starting with the oldest

(DEM_2) until the most recent monitoring (DEM_26). The difference in the z-value was calculated:

dZ=DEM_X – DEM_X-1 (1)

where X is a number between 2 and 26. From this differential DEM the volumetric change was calculated by multiplying dZ with the gully area; at 1 mm resolution. The sections of the gully outside of these 5 zones were not modelled and showed no visible changes such as deepening or sidewall collapse.

3. Results

3.1 Erosion controls and erosion susceptibility

The catchment covers an area of 15.07 ha and has a maximal length of 892 m. The area was reduced compared to the natural drainage basin by the construction of 2 large water diversion channels near the sandstone escarpment. Slopes in the catchment are generally below 0.25 m m^{-1} but exceed 1.70 m m^{-1} near the sandstone escarpment. The topography showed limited concavities which would create runoff concentration. However, one footpath running through the catchment concentrates most of the runoff from the plots above and directs it to the grassland above the gully head. The catchment has an average stone bund density of 326 m ha^{-1}. This lowered the slope length significantly to a maximum of 30 m on Vertisol compared to the absence of stone bunds in some fields on the sandy soil which creates longer continuous slopes up to 50 m. On the Vertisol, the average direction of ploughing deviated 8 degrees from contour lines. In the sandy soils downslope of the sandstone escarpment, the average tillage direction deviated 10 degrees from contour lines. These values indicate that farmers try to achieve contour ploughing.

Cite as Lannoeye, W., Stal, C., Guyassa, E., Zenebe, A., Nyssen, J., Frankl, A., 2016. The use SfM-photogrammetry to quantify and understand gully degradation at the temporal scale of rainfall events: an example from the Ethiopian drylands. Physical Geography, 37(6): 430-451. DOI 10.1080/02723646.2016.1234197.

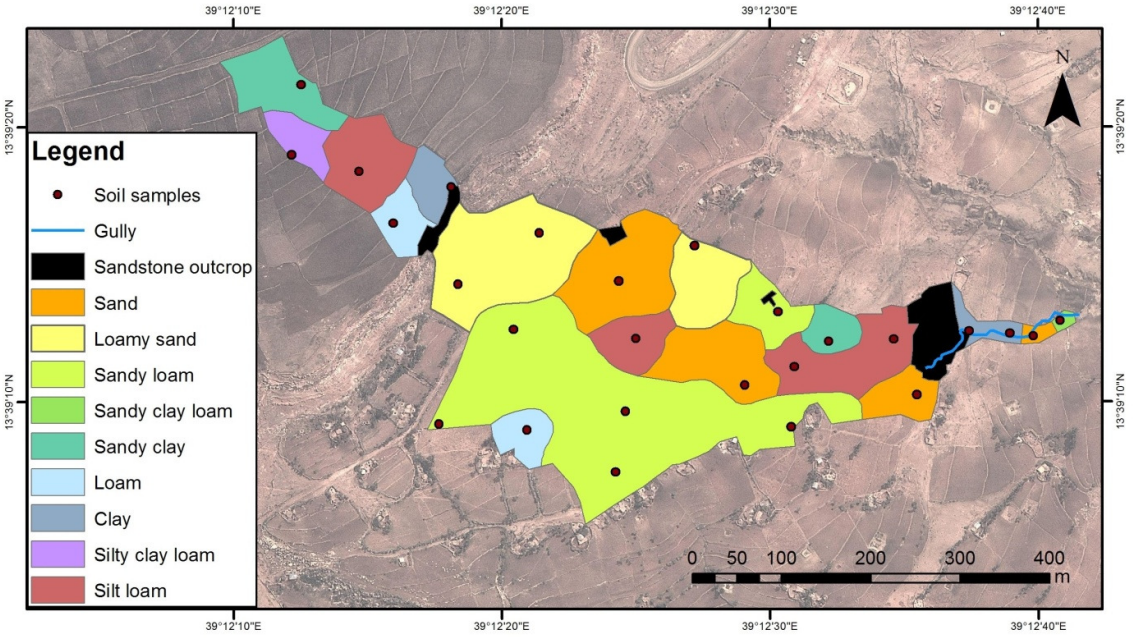

Figure 4: The soil texture map of the catchment as determined from undisturbed soil samples and observations in the catchment.

The dominant texture in the catchment was sandy loam (Figure 4), and the average sand, silt and clay contents in the catchment are respectively 50%, 30% and 20%. Below the sandstone escarpment a belt of sandier soils were found. The heavy clay Vertisols on top of the sandstone escarpment as well as the sandstone escarpment were the most important runoff production areas. However, the sandier soils below the sandstone escarpment, where infiltration capacity is much higher, excessive runoff partially infiltrated into the soil. Near the studied gully segments, the silt/clay ratio was low (0.52 ±0.21), which decreases the erodibility of the soil near the gully (Bouyoucos, 1935; Egashlra, Kaetsu & Takuma, 1983). The soil bulk density in the catchment varied between 0.98 and 1.81 g cm^{-3} with an average of 1.43 g cm^{-3} (±0.25 g cm^{-3}). The sandy soils near the gully had higher soil bulk densities than the clay soils higher up in the catchment because the latter were swollen due to antecedent rainfall. The average soil roughness for the 37 measurements was 4.86 cm (±1.80 cm). A Moran's I-index for spatial autocorrelation indicates a randomly distributed soil roughness in the catchment. The average stone cover of the soil in the catchment is 20% (±13%).

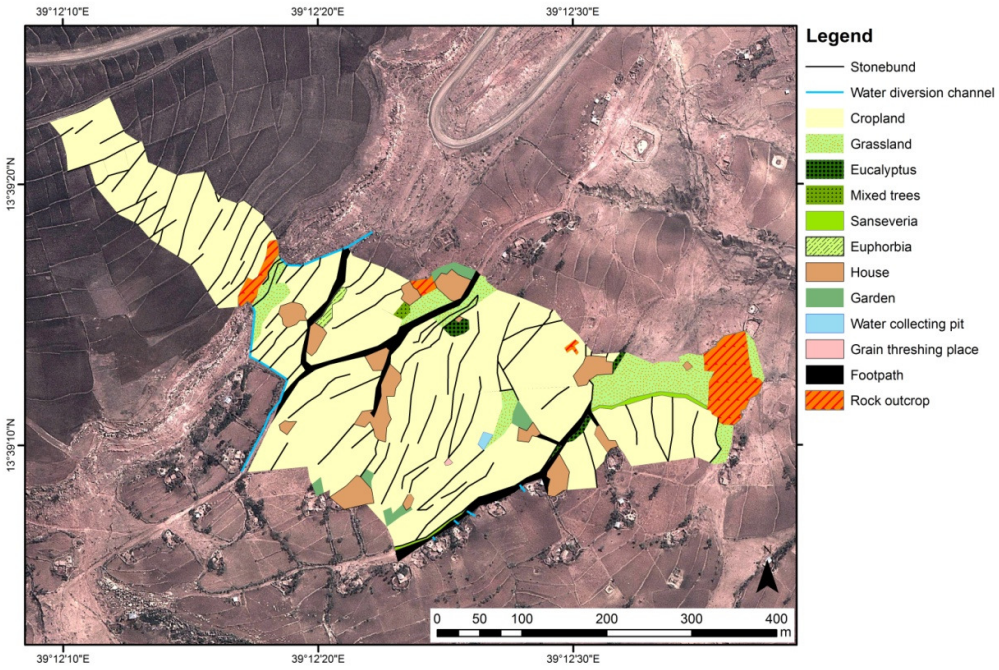

Figure 5: Land use and land management in the catchment, mapped during the summer of 2014.

The dominant land use is cropland (74.4%) (Figure 5), mostly wheat and barley, followed by grassland (7.7%) which is severely degraded by overgrazing by sheep and cattle. The cropland in the study area is primarily used for growing grains (75%). Crop height changed on average from 0.17 m on 1 August to 0.50 m on 31 August. Over the same period, the area weighted average crop cover increased to 68% (maximum cover) (Table 1, Figure 5). Interpolated crop cover showed no significant effect on runoff production (R^2=-0.01, α=0.01), No fallow croplands were observed.

During the gully monitoring period, total precipitation was 399.4 mm. The seasonal precipitation (until September 24) was 472 mm, which can be considered as a normal to normal-dry rainfall year (Frankl et al., 2013). Daily precipitation was on average 7.9 mm d^{-1} and varied between 0.2 and 54.8 mm d^{-1} (Table 1, Figure 6). 99.4% of the precipitation had an intensity lower than 30 mm h^{-1}, and one (extreme) event had a rainfall intensity of 37.8 mm h^{-1} (on 26/08/2014). Runoff occurred during 42% of the rainfall events, with a rainfall threshold of 4 mm d^{-1} and 4 mm h^{-1}. Average daily runoff depth was 1.2 mm d^{-1}, ranging between 0.2

Cite as Lannoeye, W., Stal, C., Guyassa, E., Zenebe, A., Nyssen, J., Frankl, A., 2016. The use SfM-photogrammetry to quantify and understand gully degradation at the temporal scale of rainfall events: an example from the Ethiopian drylands. Physical Geography, 37(6): 430-451. DOI 10.1080/02723646.2016.1234197.

and 7.4 mm d^{-1}. Daily runoff and precipitation depth were strongly correlated (R^2=0.79) (α=0.01), with an average runoff coefficient of 7.3% (±5%), and maximum of 18.2% (Table 1, Figure 6). From field observation, Horton overland flow was determined as the major runoff generating mechanism, and 3-days antecedent rainfall (accounting for soil moisture) had no significant effect on runoff production (R^2=0.08, α=0.01). Besides the occurrence of flash floods, a seasonal spring developed upstream of site 5, indicating high water table, from 26 July up to 12 August and from 25 August until the end of the monitoring period.

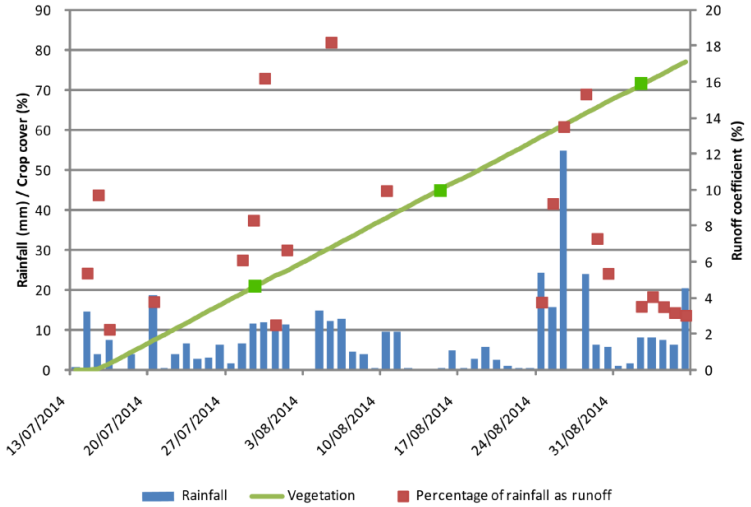

Figure 6: Vegetation growth on cropland did not show any significant impact on the runoff coefficient of the studied catchment.

Considering the erosion susceptibility of the catchment based on the RUSLE calculations, on average soil erosion rates 11.83 ton ha^{-1} y^{-1}, with 51% of the catchment having erosion rates below < 5 ton ha^{-1} y^{-1}. The most susceptible area was the rangeland above the gully head; with soil erosion rates up to 40 ton ha^{-1} y^{-1} (Figure 7). This is mainly due to the low infiltration rate, low protection to erosion by the degraded vegetation and the absence of soil management practices. Other areas with a high erosion susceptibility were the Vertisols above the sandstone escarpment (5-40 ton ha^{-1} y^{-1}). The area with sandy soils was less susceptible to erosion due to the high infiltration capacity of the soil. A zone with slightly higher erosion susceptibility central in the sandy soils is recognized in the field by a small step in the topography leading to steeper slopes. Extensive walks during and after storm events revealed no erosion features (such as rills) in the catchment; apart from the gully.

Cite as Lannoeye, W., Stal, C., Guyassa, E., Zenebe, A., Nyssen, J., Frankl, A., 2016. The use SfM-photogrammetry to quantify and understand gully degradation at the temporal scale of rainfall events: an example from the Ethiopian drylands. Physical Geography, 37(6): 430-451. DOI 10.1080/02723646.2016.1234197.

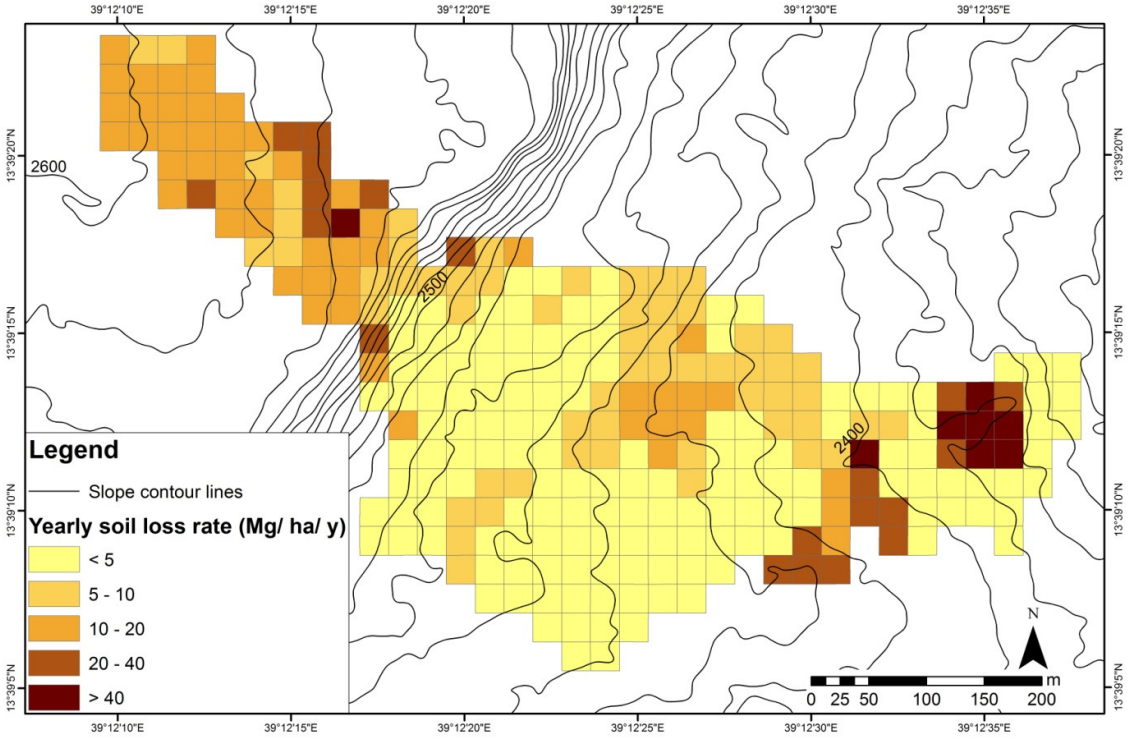

Figure 7: Erosion susceptibility of the catchment for 25 x 25m cells as calculated from the RUSLE.

3.3 Gully erosion dynamics

Both linear and volumetric retreat were considered to represent of gully erosion dynamics. Cumulative linear retreat (sum of retreat at the head cut and at the four re-incisions) occurred during eleven events, eight of which related to runoff events (Table 1). For three events, linear retreat occurred due to gravitational sidewall failures (slumping) due to undercutting after the development of a plunge pool (Figure 8a and 8b, Figure 9). Plotting cumulative linear retreat over cumulative runoff showed a strong association, with and R^2 of 0.93 (α=0.01) (Figure 10). The gully head (site 1) showed little erosion and most geomorphic change occurred at the re-incisions 3 and 4 during an extreme rainfall-runoff event on 26/08/2014.

Date	Daily Rainfall	Max. 1h Rainfall Intensity	Runoff (mm)	Runoff Coefficient (%)	Cropland Vegetation Cover (%)	Cum. Linear Retreat (m)	Cum. Volumetric Change (m)
13/07/2014	0.6	0.6				0.00	0.00
14/07/2014	14.6	14.4	0.8	5.4		0.00	0.00

15/07/2014	4.0	4	0.4	9.7		0.00	0.11
16/07/2014	7.6	6.6	0.2	2.3		0.02	-0.02
17/07/2014						0.02	-0.02
18/07/2014	4.0	2.4				0.02	-0.01
19/07/2014						0.02	-0.01
20/07/2014	18.6	9.6	0.7	3.8		0.02	0.13
21/07/2014	0.2	0.2				0.02	0.13
22/07/2014	4.0	2.8				0.02	0.13
23/07/2014	6.6	4.4				0.02	0.13
24/07/2014	2.8	1				0.02	0.13
25/07/2014	3.0	5.2				0.05	0.03
26/07/2014	6.2	3.2				0.05	0.03
27/07/2014	1.6	1.4				0.05	0.03
28/07/2014	6.6	6.6	0.4	6.1		0.06	0.03
29/07/2014	11.6	6.8	1.0	8.3		0.06	0.21
30/07/2014	12.0	10.6	1.9	16.2		0.08	0.38
31/07/2014	11.0	6.6	0.3	2.5	23.4	0.08	0.38
1/08/2014	11.2	7.8	0.7	6.7		0.10	0.36
2/08/2014						0.10	0.37
3/08/2014						0.10	0.37
4/08/2014	14.8	5.2				0.10	0.36
5/08/2014	12.2	10	2.2	18.2		0.10	0.55
6/08/2014	12.8	7.4				0.13	0.61
7/08/2014	4.6	3.8				0.14	0.63
8/08/2014	3.8	2.2				0.14	0.64
9/08/2014	0.2	0.2				0.14	0.64
10/08/2014	9.4	9.2	0.9	10.0		0.14	0.59
11/08/2014	9.4	6.8				0.15	0.65
12/08/2014	0.4	0.2				0.15	0.65
13/08/2014						0.15	0.65
14/08/2014						0.15	0.65
15/08/2014	0.2	0.2			45.1	0.15	0.65
16/08/2014	4.8	4.4				0.15	0.65
17/08/2014	0.4	0.4				0.15	0.65
18/08/2014	2.8	2.8				0.15	0.65
19/08/2014	5.6	5.2				0.15	0.65
20/08/2014	2.6	2.2				0.15	0.65
21/08/2014	1.0	0.6				0.15	0.65
22/08/2014	0.4	0.2				0.15	0.65
23/08/2014	0.2	0.2				0.15	0.65
24/08/2014	24.2	12	0.9	3.8		0.15	0.52
25/08/2014	15.6	15.4	1.4	9.3		0.18	0.51
26/08/2014	54.8	37.8	7.4	13.5		0.58	1.73
27/08/2014						0.58	1.73
28/08/2014	23.8	12.6	3.7	15.3		0.58	1.89
29/08/2014	6.4	6.2	0.5	7.3		0.58	1.86
30/08/2014	5.6	5.2	0.3	5.4		0.59	1.89
31/08/2014	1.0	0.6			68.4	0.59	1.89
1/09/2014	1.6	1.6				0.59	1.89
2/09/2014	8.0	7.2	0.3	3.5		0.59	1.97
3/09/2014	8.2	4.8	0.3	4.1		0.60	1.97
4/09/2014	7.6	6	0.3	3.5		0.60	1.97
5/09/2014	6.2	5.6	0.2	3.2		0.60	1.92

Cite as Lannoeye, W., Stal, C., Guyassa, E., Zenebe, A., Nyssen, J., Frankl, A., 2016. The use SfM-photogrammetry to quantify and understand gully degradation at the temporal scale of rainfall events: an example from the Ethiopian drylands. Physical Geography, 37(6): 430-451. DOI 10.1080/02723646.2016.1234197.

6/09/2014	20.4	15.2	0.6	3.1	0.60	2.04
7/09/2014	4.2	2.8			0.60	2.04
8/09/2014	4.6	3.4			0.60	2.04

Table 1: Rainfall, runoff, vegetation growth and gully erosion dynamics

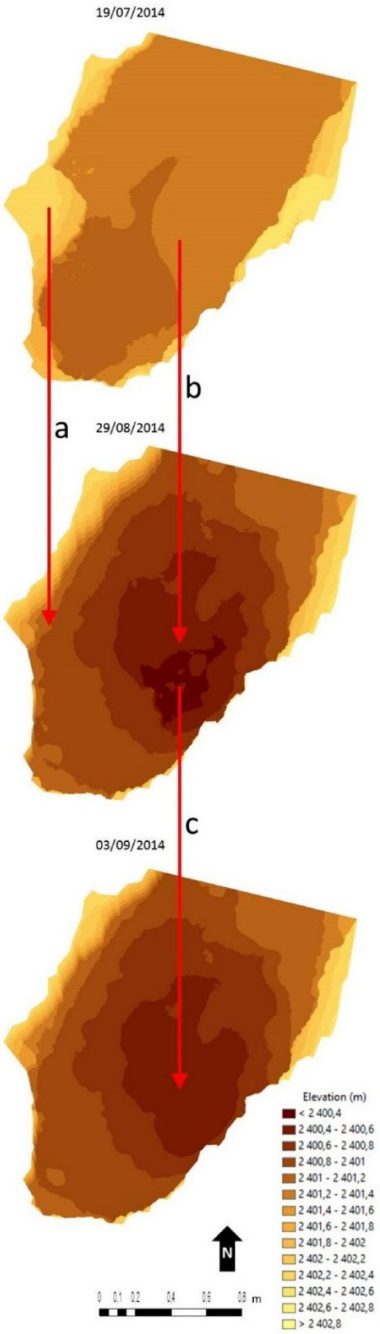

Figure 8: Erosion dynamics as studied from multi-temporal DEMs for re-incision 4: (A) slumping, (B) plunge pool erosion, (C) sediment deposition (The water flows from SW to NE).

Volumetric gully erosion dynamics in the five monitored gully segments were complex, with both gully degradation and gully infilling occurring, often asynchronous between sites (Figure 11, Table 1). Considering cumulative volumetric changes, besides gully degradation by sidewall erosion and plunge pool erosion, gully floor sedimentation (Figure 8c, Figure 9) of the plunge pool during small runoff events, also caused cumulative filling of the gully (Table 1, Figure 8 and 9).

Figure 9: (A) Unconcentrated runoff in the catchment on compacted grassland just above the gully head; (B) Concentrated runoff at incision 4 causing plunge pool erosion (gully head is 1.2 m across); (C) Dispersed runoff between incision 4 and 5 causing sedimentation.

The most dynamic site was the re-incision at site 4, which had volumetric changes during al runoff events; with erosion rates usually increasing with stronger runoff events. Here also,

Cite as Lannoeye, W., Stal, C., Guyassa, E., Zenebe, A., Nyssen, J., Frankl, A., 2016. The use SfM-photogrammetry to quantify and understand gully degradation at the temporal scale of rainfall events: an example from the Ethiopian drylands. Physical Geography, 37(6): 430-451. DOI 10.1080/02723646.2016.1234197.

most geomorphic change occurred during the extreme of 26/08/2014. Over the whole period of monitoring, site 4 showed the largest volumetric change with 1.23 m³ followed by site 2 (0.23 m³), site 5 (0.16 m³), site 1 (0.07 m³) and 3 (0.01 m³). The gully head (site 1) experienced only minor changes compared to the lower re-incisions, partly explained by the incision in bedrock. The deposition of the sand between sites 4 and 5 could be explained by the lowering of the velocity in this part of the stream due to widening of the streambed (Andrews, 1978). Towards site 5 the stream concentrates again and gains velocity.

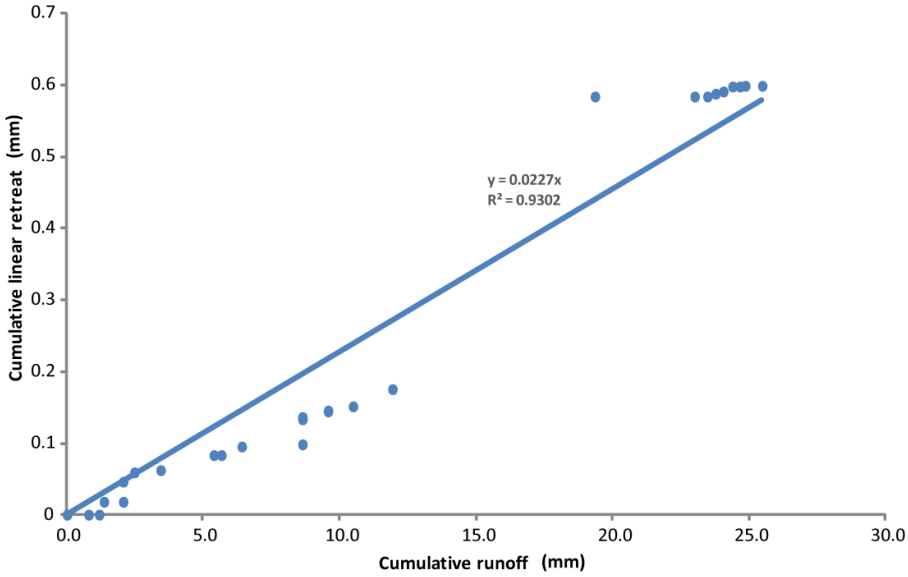

Figure 10: Cumulative rainfall versus cumulative linear retreat showing the strong relationship between both and the important effect of extreme events.

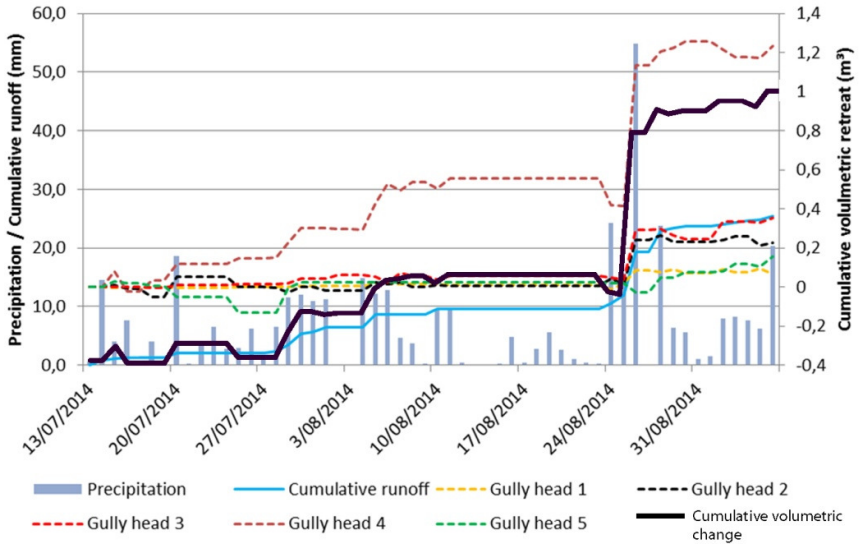

Cite as Lannoeye, W., Stal, C., Guyassa, E., Zenebe, A., Nyssen, J., Frankl, A., 2016. The use SfM-photogrammetry to quantify and understand gully degradation at the temporal scale of rainfall events: an example from the Ethiopian drylands. Physical Geography, 37(6): 430-451. DOI 10.1080/02723646.2016.1234197.

Figure 11: Precipitation, Cumulative runoff and cumulative absolute volumetric change (degradation and aggradation) at the study site in Adi Kolkwal quantified from DEMs created with Photoscan.

Cite as Lannoeye, W., Stal, C., Guyassa, E., Zenebe, A., Nyssen, J., Frankl, A., 2016. The use SfM-photogrammetry to quantify and understand gully degradation at the temporal scale of rainfall events: an example from the Ethiopian drylands. Physical Geography, DOI 10.1080/02723646.2016.1234197.

Considering all sites, a gully erosion rate of 0.19 t ha^{-1} y^{-1} was obtained, versus only 0.008 t ha^{-1} y^{-1} for the gully head alone. Strong positive correlations of volumetric retreat were observed between upper and lower sites studied (Table 2). These correlations show that a rise in sediment load by erosion in the upper head cuts have no influence on the erosion rates of the lower head cuts.

Upper gully head(s)	Lower gully head(s)	Correlation (R)
Gully head 1	Gully head 2+3+4+5	0.589**
Gully head 1+2	Gully head 3+4+5	0.839**
Gully head 1+2+3	Gully head 4+5	0.799**
Gully head 1+2+3+4	Gully head 5	-0.188

Table 2: Correlations for the change in retreat rates between the upper incision(s) and the lower incision(s).

4. Discussion

4.1 SfM-photogrammetry

As in previous research, SfM-photogrammetry could successfully be used to quantify gully morphology at high spatial resolutions (Kaiser et al., 2014; Frankl et al., 2015), whilst implementing it here at the high temporal scale of rainfall events. While images taken from a ground perspective allow to photograph and thus model the real surface topography in 3D, the large number of photographs needed and the time required to survey large areas limit the use of a ground-based approach to small areas. To tackle this, Stöcker et al. (2015) integrated the use of UAVs with ground-based photographs, and here, we used a camera mounted on a 5 m high wooden pole as a substitute for a UAV.

Considering data collection, the SfM-photogrammetry method is strongly depending on weather conditions. The light conditions and contrast (limiting contrasting over-exposed areas and shadow casts) of the photographed feature must be optimal, making it important to have some cloud cover during photographing, and thus limiting the time-window of the monitoring exercise. The largest challenge for SfM-MVS modelling, however, is vegetation in and near the surveyed landform. The vegetation conceals the real topography and thus needs to be clipped to the surface, which can impact gully dynamics. Although vegetation was scarce in the gully, it had to be clipped several times over the length of the rainy season.

Computational limitations are related to the available memory of the computer workstation. For a dataset between 20 and 50 photographs, the advised memory is between 32 and 96 GB for 3D model construction at the highest quality settings. When undercut features are included whilst photographing a landform, large numbers of photographs are rapidly required. This limits the possibilities to extend the model. To reduce the number of photographs for certain areas, undercut features, although important to gully erosion dynamics, can be excluded or photographs can be taken from a higher altitude (using a UAV).

4.2 Catchment characteristics and erodibility

The results for the RUSLE revealed a low erodibility of the catchment (average 11.83 ton ha^{-1} y^{-1}; < 5 ton ha^{-1} y^{-1} for 51 % of the catchment), lower than the nearby catchment of May Zeg Zeg studied 7 years ago (Nyssen et al., 2009). These low values are the result of the successful implementation of soil management measures (e.g. stone bunds, contour ploughing), and reflect the huge conservation efforts made in the region (Taye et al., 2013; Frankl et al., 2011). Main explanatory variables for the low erodibility are the tillage direction which is approximately following the contour of the slope (Takken et al., 2001; Gebreegziabher et al., 2009), the implementation of stone bunds (Taye et al., 2013), and the high crop cover (Zhou, Luukkanen, Tokola & Nieminnen, 2008). Averaged over the entire catchment the silt/clay ratio is small (0.52 ±0.221), while near the gully it is relatively high (2.22 ±1.66). Four soil samples have a silt/clay ratio bigger than four which suggests these soils are very prone to erosion (Bouyoucous, 1935; Egashlra et al., 1983). The somewhat higher results for the RUSLE above the sandstone escarpment are mainly due to the presence of Vertisols. Near the gully, high values for erodibility can be found on the degraded rangeland where no erosion control measures are present, and therefore, new efforts should concentrate on this area; typically left unmanaged since the threat of gully erosion is apparent. While the results for the arable land show an improvement compared to the study of Nyssen et al. (2009), the rangeland performs worse, indicating that overgrazing remains a major challenge.

4.3 Retreat rates compared to other research

The study of gully degradation mainly focuses on the gully head cuts (Vanmaercke et al., 2016). However, from this study, studying only the uppermost incision of gullies limits the understanding of gully erosion dynamics and rates. While the gully head can be relatively

stable, re-incision at lower locations can still cause important gully degradation, which ultimately will reach the gully head and cause instability. Also, this event-based monitoring demonstrated that gully degradation was mainly caused by one major rainfall event (26/08/2016, 54.8 mm d^{-1}), and that smaller rainfall-runoff events result in complex degradation and/or aggradation along the gully channel; which aligns these findings with precious research (Frankl et al., 2012; Marzolff, Ries & Poesen, 2011).

Headcut erosion rates of this study are low compared to others measured in Ethiopia (Nyssen et al., 2004a; Frankl et al., 2012) and Kenia (Oostwoud Wijdenes and Bryan 2001) but similar compared to retreat rates in Spain (Vandekerckhove, Poesen, Oostwoud-Wijdenes & Gyssels, 2001; Vandekerckhove, Poesen & Govers, 2003) (Table 3). The main explanation for this are the soil and land management practices implemented in the catchment. Finally, the impact of soil characteristics such as soil moisture and infiltration capacity is not explicitly studied here but could have an additional explanatory factor in the rainfall-runoff relations in the catchment.

Retreat rates per ha	Volumetric retreat (m^3 ha^{-1} y^{-1})
This research	0.41
Nyssen et al. (2002)	65.26
Frankl et al. (2012) (short term)	0.90
Frankl et al. (2012) (medium/long term)	0.82
Oostwoud Wijdenes and Bryan (2001)	6.61
Vandekerckhove et al. (2001)	0.10
Vandekerckhove et al. (2003)	0.51

Table 3: Values normalised for catchment area for head cut retreat rates.

5. Conclusions

In this study, we demonstrated the use of SfM-photogrammetry at both high spatial and temporal scales to study gully erosion dynamics for a gully in the drylands of Northern Ethiopia. Considering the use of SfM-photogrammetry (and thus multi-temporal DEMs) to study gully dynamics at the temporal scale of rainfall events, although the method is cost-efficient and flexible, terrestrial approaches (required to model the real surface topography) limit the spatial extend of the study as the method is time consuming and large computational

resources are required when modelling terrain features. To tackle this, terrestrial approaches may be combined with aerial approaches such as the use of UAVs, or as done here a camera mounted on a pole.

Considering the erodibility of the catchment, this study confirms that indeed, the huge efforts in soil and water conservation are paying off, with low values obtained from the application of the RUSLE (average of 11.83 ton ha^{-1} y^{-1}). Critical locations in the landscape, such as the area just above the gully head are, however, poorly managed, probably because local societies assess that the land is already lost. Gully degradation (studied here from the gully head and four re-incisions) mainly occurred during runoff events, which was strongly correlated to daily precipitation, with a rainfall threshold for runoff production of 4 mm d^{-1}. However, slumping of gully banks also occurred on dry days. Gully degradation during consecutive runoff events (mainly by plunge pool development) could be demonstrated from the multi-temporal DEMs, and indicate that the major geomorphic change was the result of one major rainfall event on 26/08/2014, when the daily precipitation was 54.8 mm. Important is that although most research focusses on gully heads alone, re-incisions at lower locations can still cause important gully degradation, which ultimately will reach the gully head and cause instability. This is well demonstrated by the erosion rate, which was 0.19 t ha^{-1} y^{-1} for all the incision combined, compared to 0.008 t ha^{-1} y^{-1} for the gully head alone.

Acknowledgments

This study was partially funded with a VLIR-UOS travel grant of Wouter Lannoeye. We thank Gebrekidan Mesfin for assistance in the field and the VLIR-UOS team at Mekelle University for logistical support. Many thanks go to the helpful villagers of Adi Kolkwal and to the Gitbadik family for providing accommodation near the catchment. Thanks also to the anonymous reviewers for their comments and suggestions in improving this manuscript.

References

Andrews, E. D. (1979). *Scour and fill in a stream channel*, *East Fork River, Western Wyoming* (No. 1117). US Government Printing Office.

Betts, H. D., Trustrum, N. A., & Rose, R. C. D. (2003). Geomorphic changes in a complex gully system measured from sequential digital elevation models, and implications for management. *Earth Surface Processes and Landforms*, 28(10), 1043-1058.

Cite as Lannoeye, W., Stal, C., Guyassa, E., Zenebe, A., Nyssen, J., Frankl, A., 2016. The use SfM-photogrammetry to quantify and understand gully degradation at the temporal scale of rainfall events: an example from the Ethiopian drylands. Physical Geography, DOI 10.1080/02723646.2016.1234197.

Bonilla, E. A. F., Sheehan, A., & Tucker, G. (2008). Terrestrial Laser Scanning Study of Gully Erosion at West Bijou Creek, Arapahoe County, Colorado: An Investigation on Field Acquisition and Data Processing. In *AGU Fall Meeting Abstracts* (Vol. 1, p. 635).

Bouyoucos, G.J. (1935) The clay ratio as a criterion of susceptibility of soils to erosion. *Journal of the American Society of Agronomy.* 27, 738-741.

Burkard, M. B., & Kostaschuk, R. A. (1995). Initiation and evolution of gullies along the shoreline of Lake Huron. *Geomorphology*, 14(3), 211-219.

Burkard, M. B., & Kostaschuk, R. A. (1997). Patterns and controls of gully growth along the shoreline of Lake Huron. *Earth Surface Processes and Landforms*, *22*(10), 901-911.

Castillo, C., Pérez, R., James, M. R., Quinton, J. N., Taguas, E. V., & Gómez, J. A. (2012). Comparing the accuracy of several field methods for measuring gully erosion. *Soil Science Society of America Journal*, 76(4), 1319-1332.

de Mûelenaere, S., Frankl, A., Mitiku Haile, Poesen, J., Deckers, J., Munro, R.N., Veraverbeke, S. & Nyssen, J. (2014). Historical landscape photographs for calibration of Landsat land use/cover (1972) in the northern Ethiopian highlands. *Land Degradation & Development*, 25 (4): 319-335.

Dinssa, E. G., Frankl, A., Degefa, A. Z., Poesen, J., & Nyssen, J. (2015). Effect of check dams in gullies on runoff response in the headwaters of Tekeze reservoir. *TropiLakes 2015 international conference on tropical lakes in a changing environment: water, land, biology, climate and humans*, 80.

d'Oleire-Oltmanns, S., Marzolff, I., Peter, K. D., & Ries, J. B. (2012). Unmanned Aerial Vehicle (UAV) for monitoring soil erosion in Morocco. *Remote Sensing*, 4(11), 3390-3416.

Egashlra, K., Kaetsu, Y., & Takuma, K. (1983). Aggregate stability as an index of erodibility of Ando soils. *Soil science and plant nutrition*, 29(4), 473-481.

FAO. (2011). *The state of the world's land and water resources for food and agriculture (SOLAW) – Managing systems at risk*. Food and Agriculture Organization of the United Nations, Rome and Earthscan, London.

Frankl, A., Jacob, M., Haile, M., Poesen, J., Deckers, J. & Nyssen, J. (2013). The effect of rainfall on the spatio-temporal variability of cropping systems and duration of the crop cover in the Northern Ethiopian Highlands. *Soil Use and Management* 29 (3), 374-383

Frankl, A., Nyssen, J., De Dapper, M., Haile, M., Billi, P., Munro, R. N., Deckers, J. & Poesen, J. (2011). Linking long-term gully and river channel dynamics to environmental

change using repeat photography (Northern Ethiopia). *Geomorphology*, 129(3), 238-251.

Frankl, A., Poesen, J., Deckers, J., Haile, M., & Nyssen, J. (2012). Gully head retreat rates in the semi-arid highlands of Northern Ethiopia. *Geomorphology*, 173, 185-195.

Frankl, A., Stal, C., Abraha, A., Nyssen, J., Rieke-Zapp, D., De Wulf, A., & Poesen, J. (2015). Detailed recording of gully morphology in 3D through image-based modelling. *Catena*, 127, 92-101.

Gebremedhin, B. & Swinton, S.M. (2003). Investment in soil conservation in northern Ethiopia: the role of land tenure security and public programs. *Agricultural Economics* 29, 69–84.

Gómez-Gutiérrez, Á., Schnabel, S., Berenguer-Sempere, F., Lavado-Contador, F., & Rubio-Delgado, J. (2014). Using 3D photo-reconstruction methods to estimate gully headcut erosion. *Catena*, 120, 91-101.

Heritage, G., & Hetherington, D. (2007). Towards a protocol for laser scanning in fluvial geomorphology. *Earth Surface Processes and Landforms*, 32(1), 66-74.

Hu, G., Wu, Y., Liu, B., Yu, Z., You, Z., & Zhang, Y. (2007). Short-term gully retreat rates over rolling hill areas in black soil of Northeast China. *Catena*, 71(2), 321-329.

James, M. R., & Varley, N. (2012). Identification of structural controls in an active lava dome with high resolution DEMs: Volcán de Colima, Mexico. *Geophysical Research Letters*, 39(22).

James, M. R., Ilic, S., & Ruzic, I. (2013). Measuring 3D coastal change with a digital camera. In Green, A. & Cooper, J. (Eds). *Proceedings of the 7th International Conference on Coastal Dynamics.* Bordeaux: Université de Bordeaux: pp. 24-28.

Javernick, L., Brasington, J., & Caruso, B. (2014). Modeling the topography of shallow braided rivers using Structure-from-Motion photogrammetry. *Geomorphology*, 213, 166-182.

Kaiser, A., Neugirg, F., Rock, G., Müller, C., Haas, F., Ries, J., & Schmidt, J. (2014). Small-Scale Surface Reconstruction and Volume Calculation of Soil Erosion in Complex Moroccan Gully Morphology Using Structure-from-Motion. *Remote Sensing*, 6(8), 7050-7080.

Kociuba, W., Janicki, G., & Rodzik, J. (2014). 3D laser scanning as a new tool of assessment of erosion rates in forested loess gullies (case study: Kolonia Celejów, Lublin Upland). *Annales UMCS, Geographia, Geologia, Mineralogia et Petrographia*, 69(1), 107-116.

Lanckriet, S., Derudder, B., Naudts, J., Bauer, H., Deckers, J., Haile, M., & Nyssen, J. (2014). A political ecology perspective of land degradation in the north Ethiopian highlands. *Land Degradation & Development*, 26(5), 521-530.

Lucieer, A., de Jong, S., & Turner, D. (2013). Mapping landslide displacements using Structure-from-Motion (SfM) and image correlation of multi-temporal UAV photography. *Progress in Physical Geography*, 1-20.

Marzolff, I., Ries, J. B., & Poesen, J. (2011). Short-term versus medium-term monitoring for detecting gully-erosion variability in a Mediterranean environment. *Earth Surface Processes and Landforms*, 36(12), 1604-1623.

Meire, E., Frankl, A., De Wulf, A., Mitiku Haile, Deckers, J. & Nyssen, J. (2013). Land use and cover dynamics in Africa since the 19th century - warped terrestrial photographs of North Ethiopia. *Regional Environmental Change* 13 (3): 717-737.

Ndona, A., Truong, P., 2011. Community mobilization for the control of ravine erosion with vetiver technology in the Congo, http://www.vetiver.org/ICV4pdfs/DC04.pdf. 2011 (last accessed on 14 July 2015).

Nyssen, J., Veyret Picot, M., Poesen, J., Moeyersons, J., Mitiku, H., Deckers, J., Govers, G., (2004a). The effectiveness of loose rock check dams for gully control in Tigray, northern Ethiopia. *Soil Use and Management*, 20 (1), 55–64.

Nyssen, J., Poesen, J., Moeyersons, J., Deckers, J., Mitiku, H., Lang, A., (2004b). Human impact on the environment in the Ethiopian and Eritrean highlands - a state of the art. *Earth Science Reviews*, 64 (3–4), 273– 320.

Nyssen, J., Vandenreyken, H., Poesen, J., Moeyersons, J., Deckers, J., Haile, M., Salles, C. & Govers, G. (2005). Rainfall erosivity and variability in the Northern Ethiopian Highlands. *Journal of Hydrology*, 311(1), 172-187.

Nyssen, J., Poesen, J., Veyret-Picot, M., Moeyersons, J., Haile, M., Deckers, J., Dewit, J., Naudts, J. Teka, K., Govers, G. (2006). Assessment of gully erosion rates through interviews and measurements: a case study from Northern Ethiopia. Earth Surface Processes and Landforms, 31(2), 167-185.

Nyssen, J., Poesen, J., Haile, M., Moeyersons, J., Deckers, J., & Hurni, H. (2009). Effects of land use and land cover on sheet and rill erosion rates in the Tigray highlands, Ethiopia. *Zeitschrift für Geomorphologie*, 53(2), 171-197.

Oostwoud Wijdenes, D. J., Poesen, J., Vandekerckhove, L., Nachtergaele, J., & De Baerdemaeker, J. (1999). Gully-head morphology and implications for gully

development on abandoned fields in a semi-arid environment, Sierra de Gata, southeast Spain. *Earth Surface Processes and Landforms*, 24(7), 585-603.

Oostwoud Wijdenes, D. J., & Bryan, R. (2001). Gully-head erosion processes on a semi-arid valley floor in Kenya: a case study into temporal variation and sediment budgeting. *Earth Surface Processes and Landforms*, 26(9), 911-933.

Perroy, R. L., Bookhagen, B., Asner, G. P., & Chadwick, O. A. (2010). Comparison of gully erosion estimates using airborne and ground-based LiDAR on Santa Cruz Island, California. *Geomorphology*, 118(3), 288-300.

Peter, K. D., d'Oleire-Oltmanns, S., Ries, J. B., Marzolff, I., & Hssaine, A. A. (2014). Soil erosion in gully catchments affected by land-levelling measures in the Souss Basin, Morocco, analysed by rainfall simulation and UAV remote sensing data. *Catena*, 113, 24-40.

Poesen, J., Nachtergaele, J., Verstraeten, G., Valentin, C. (2003). Gully erosion and environmental change, importance and research needs. *Catena*, 50, 91–133.

Remondino, F., & El-Hakim, S. (2006). Image-based 3D Modelling: A Review. *The Photogrammetric Record*, 21(115), 269-291.

Robinson, P.J. & Henderson-Sellers, A. (1999). Contemporary Climatology. Pearson Education Ltd., Essex.

Rothmund, S., Niethammer, U., Malet, J. P., & Joswig, M. (2013). Landslide surface monitoring based on UAV-and ground-based images and terrestrial laser scanning:

Schumm, S. A. (2005). *River variability and complexity*. Cambridge University Press.

Soil Survey Division Staff (1993). *Soil survey manual*. Soil Conservation Service. U.S. Department of Agriculture Handbook 18.

Stöcker, C., Eltner, A., & Karrasch, P. (2015). Measuring gullies by synergetic application of UAV and close range photogrammetry - A case study from Andalusia, Spain. *Catena*, 132, 1-11.

Taye, G., Poesen, J., van Wesemael, B., and 8 others (2013). Effects of land use, slope gradient, and soil and water conservation structures on runoff and soil loss in semi-arid Northern Ethiopia. Physical Geography Volume 34, Issue 3, June 2013, pages 236-259.

Thomsen, L., Stolte, J., Baartman, J., & Starkloff, T. (2014, May). Soil roughness: comparing old and new methods and application in a soil erosion model. In *EGU General Assembly Conference Abstracts*, 16, 5558.

Valentin, C., Poesen, J., & Li, Y. (2005). Gully erosion: impacts, factors and control. *Catena*, 63(2), 132-153.

Vandekerckhove, L., Poesen, J., Wijdenes, D. O., & Gyssels, G. (2001). "Short-term bank gully retreat rates in Mediterranean environments". *Catena*, 44(2), 133-161.

Vandekerckhove, L., Poesen, J., & Govers, G. (2003). "Medium-term gully headcut retreat rates in Southeast Spain determined from aerial photographs and ground measurements". *Catena*, 50(2), 329-352.

Vanmaercke, M., Poesen, J., Van Mele, B., Demuzere, M., Bruynseels, A., Golosov, V., Rodigues Bezerra, J.F., Bolysov, S., Dvinskih, A., Frankl, A., Fuseina, Y., Guerra, A., Haregeweyn, N., Ionita, I., Makanzu Imwangana, F., Moeyersons, J., Moshe, I., Nazari Samani, A., Niascu, L., Nyssen, J., Otsuki, Y., Radoane, M., Rysin, I., Ryzhov, Y.V., Yermolaev, O., (2016). How fast do hully headcuts retreat? Earth-Science Reviews 154, 336-335.

Vanwalleghem, T., Bork, H. R., Poesen, J., Schmidtchen, G., Dotterweich, M., Nachtergaele, J., Bork, H., Deckers, J., Brüsch, B. Bungeneers, J., De Bie, M. (2005). Rapid development and infilling of a buried gully under cropland, central Belgium. *Catena*, 63(2), 221-243.

Verhoeven, G. (2011). Taking computer vision aloft–archaeological three-dimensional reconstructions from aerial photographs with Photoscan. *Archaeological Prospection*, 18(1), 67-73.

Westoby, M. J., Brasington, J., Glasser, N. F., Hambrey, M. J., & Reynolds, J. M. (2012). 'Structure-from-Motion'photogrammetry: A low-cost, effective tool for geoscience applications. *Geomorphology*, 179, 300-314.

Wu, Y., & Cheng, H. (2005). Monitoring of gully erosion on the Loess Plateau of China using a global positioning system. *Catena*, 63(2), 154-166.

Zhou, P., Luukkanen, O., Tokola, T., & Nieminen, J. (2008). Effect of vegetation cover on soil erosion in a mountainous watershed. *Catena*, 75(3), 319-325.

Cite as Lannoeye, W., Stal, C., Guyassa, E., Zenebe, A., Nyssen, J., Frankl, A., 2016. The use SfM-photogrammetry to quantify and understand gully degradation at the temporal scale of rainfall events: an example from the Ethiopian drylands. Physical Geography, DOI 10.1080/02723646.2016.1234197.

278

Cite as Lannoeye, W., Stal, C., Guyassa, E., Zenebe, A., Nyssen, J., Frankl, A., 2016. The use SfM-photogrammetry to quantify and understand gully degradation at the temporal scale of rainfall events: an example from the Ethiopian drylands. Physical Geography, DOI 10.1080/02723646.2016.1234197.

279